Reprinted from APPLIED OPTICS, Vol. 21, page 147, January 1, 1982

Microprocessor-based fiber-optic iterative optical processor

Mark Carlotto and David Casasent

The design and fabrication of an iterative optical vector–matrix processor are described. Microprocessor feedback is used to produce an iterative processor capable of solving simultaneous linear equations. It also facilitates scaling and biasing of the data and the handling of bipolar and complex-valued data as well as correction for selected system error sources. Fiber-optic interconnections are used to improve the system's alignment and to reduce its size, weight, and errors. The design, fabrication, and performance of the system are analyzed.

I. Introduction

Optical vector–matrix multipliers[1-3] represent a general class of optical processors since many data processing problems can be formulated as vector–matrix equations or as a set of simultaneous linear algebraic equations. One of the most attractive ways to realize an optical vector–matrix multiplier with present-day hardware is to image a linear array of LEDs through a 2-D mask and onto a linear photodetector array.[3] Both serial systems[4,5] using one LED (whose output is time-sequentially modulated) and parallel systems[6,7] (with a linear array of input LEDs) have been described to achieve an optical vector–matrix multiplication. In both cases, the LED outputs describe the elements of a vector, the transmittances of the 2-D mask describe the elements of a matrix, and the system's output is a vector–matrix product. With a 2-D output CCD shift register detector, one can perform convolutions on such a system.[5] When the transmittances of the mask elements correspond to the Fourier kernels, the outputs on the linear photodetector array are the discrete Fourier transform of the sampled input data present on the linear LED input array.[6]

In Ref. 8 we described an iterative optical processor (IOP) in which the linear photodetector outputs from a vector–matrix multiplier were combined with an external vector, and the result fed back to the linear LED inputs. The use of this system in adaptive phased array radar processing,[9] eigenvalue and eigenvector computation,[10,11] and for optimal control applications[12] has been described. In the course of these application studies increasingly complex operations and control were required in the electronic feedback loop, and more attention to the system's accuracy was necessitated. In this paper, we describe the microprocessor-based fiber-optic IOP system we designed and fabricated to address future applications. In Sec. II we describe the new iterative algorithm we use with emphasis on the algorithm's convergence. Scaling, biasing, and how bipolar and complex-valued data are handled on the system are described in Sec. III. Following a description of the microprocessor-based fiber-optic IOP system we designed and fabricated (Sec. IV), an error analysis and quantification of the laboratory system's performance are advanced in Sec. V.

II. Convergence of the Iterative Algorithm

In Fig. 1 we show a simplified schematic diagram of the IOP. Bipolar-valued matrices are denoted by $\mathbf{H}$ and bipolar-valued vectors by $\mathbf{y}$ and $\mathbf{x}$. These are distinguished from the vector and matrix quantities ($\mathbf{a}$,$\mathbf{c}$,$\mathbf{B}$) in the physical optical system. This is necessary, since the latter must be real and positive. Complex-valued quantities will be denoted by a tilde above the variable. Considering the physical system first, we denote the light distribution leaving the linear input LED array at $\mathbf{P}_1$ at iteration j by the vector $\mathbf{a}^T(j)$ with elements $a_m(j)$. The light distribution leaving $\mathbf{P}_1$ is imaged vertically and expanded horizontally to uniformly illuminate the rows of the mask at $\mathbf{P}_2$ with light from the corresponding input LED. We denote the transmittance of the mask at $\mathbf{P}_2$ by the matrix $\mathbf{B}^T$ with elements b_{mn}. The light

When this work was done both authors were with Carnegie-Mellon University, Department of Electrical Engineering, Pittsburgh, Pennsylvania 15213; M. Carlotto is now with Analytical Sciences Corporation, 1 Jacob Way, Reading, Massachusetts 01867.

Received 24 July 1981.
0003-6935/82/010147-06$01.00/0.

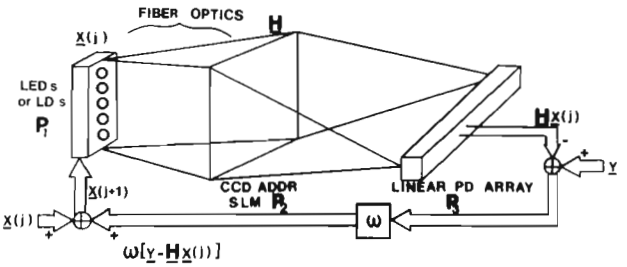

Fig. 1. Schematic diagram of the IOP emphasizing the iterative algorithm.

distribution leaving each column of $\mathbf{P}_2$ is summed on the corresponding photodetector and the linear output detector array at $\mathbf{P}_3$. The system's output is thus the vector–matrix product $\mathbf{c}^T(j) = \mathbf{a}^T(j)\mathbf{B}^T$. For notational simplicity, we will suppress the use of transposed vectors and matrices and thus describe the vector–matrix product by

$$\mathbf{c}(j) = \mathbf{B}\mathbf{a}(j), \tag{1}$$

with elements

$$c_n = \sum_{m=1}^{M} a_m b_{mn}, \tag{2}$$

where $\mathbf{c}$ has N elements, $\mathbf{a}$ has M elements, and $\mathbf{B}$ is an $M \times N$ matrix.

If the light distribution leaving the LEDs at $\mathbf{P}_1$ at iteration j is $\mathbf{x}(j)$, and the mask transmittance is described by $\mathbf{H}$, the output from the photodetectors at $\mathbf{P}_3$ is $\mathbf{H}\mathbf{x}(j)$. We form the difference between this output and a fixed external vector $\mathbf{y}$, multiply the difference by an acceleration parameter ω, and add the result to the original input vector $\mathbf{x}(j)$ to form a new $\mathbf{x}(j+1)$ input for iteration $j+1$. The system thus realizes the Richardson algorithm[13]

$$\mathbf{x}(j+1) = \mathbf{x}(j) + \omega[\mathbf{y} - \mathbf{H}\mathbf{x}(j)]. \tag{3}$$

When $\mathbf{x}(j) \cong \mathbf{x}(j+1) = \mathbf{x}$, Eq. (3) reduces to

$$\mathbf{H}\mathbf{x} = \mathbf{y}, \tag{4}$$

and the system's output

$$\mathbf{x} = \mathbf{H}^{-1}\mathbf{y} \tag{5}$$

is the desired solution to the vector–matrix equation in Eq. (4).

To insure convergence of Eq. (3) for all initializations $\mathbf{x}(0)$ of the system, the N roots $s_n(\omega)$ of the characteristic equation:

$$\text{determinant}|s\mathbf{I} - (\mathbf{I} - \omega\mathbf{H})| \tag{6}$$

of the discrete time system must lie strictly within the unit circle in the z-plane.[14] If λ_i are the eigenvalues of $\mathbf{H}$, we must satisfy

$$0 < |1 - \omega\lambda_i| < 1 \tag{7}$$

to insure convergence of Eq. (3). An obvious choice for ω is

$$\omega = -1/\lambda_{\max}, \tag{8}$$

where $\lambda_{\max}$ is the absolute value of the largest eigenvalue of $\mathbf{H}$. With ω chosen as in Eq. (8), Eq. (7) is satisfied for the largest λ_i and thus is easily satisfied for smaller λ_i values. In practice, we can increase ω slightly from the value in Eq. (8) to insure that $|1 - \omega\lambda_i| > 0$. In special cases, when highly oscillatory poles of $\mathbf{H}$ occur, we can select ω to be a multiple of $1/\lambda_{\max}$. (We have yet to consider cases when this situation arises.)

Let us now consider how to compute the choice of ω noted in Eq. (7). We generally use the conservative upper-bound[15]

$$\lambda_{\max} < ||\mathbf{H}|| = \left(\sum_m \sum_n h_{mn}^2\right)^{1/2} \tag{9}$$

for $\lambda_{\max}$. However, it is also possible to use the IOP itself to estimate $\lambda_{\max}$ as we now describe.

In this case, we let $\mathbf{y} = 0$, place $\mathbf{H}$ at $\mathbf{P}_2$, and describe the initial input vector $\mathbf{x}(0)$ at iteration $j = 0$ by

$$\mathbf{x}(0) = a_1\phi_1 + a_2\phi_2 + \ldots + a_M\phi_M, \tag{10}$$

where the ϕ_m are the eigenvectors of $\mathbf{H}$. We feed the output at each iteration directly back to the input and thus after j iterations find

$$\mathbf{x}(j) = \mathbf{H}^j\mathbf{x}(0). \tag{11}$$

We can write $\mathbf{H}$ in terms of its eigenvalues λ_m and its eigenvectors ϕ_m by singular value decomposition as

$$\mathbf{H} = \sum_m \phi_m\lambda_m\phi_m^T. \tag{12}$$

Multiplying both sides of Eq. (10) by ϕ_m^T and using the orthonormality of eigenvectors, we find $a_m = \phi_m^T\mathbf{x}(0)$. Using this in Eq. (11), we find that $\mathbf{x}(j)$ can be rewritten as

$$\mathbf{x}(j) = \sum_m \phi_m\lambda_m^j a_m. \tag{13}$$

After a sufficiently large number j of iterations, the eigenvector ϕ_d with the largest eigenvalue $\lambda_{\max}$ will dominate the summation in Eq. (13), and the system's output will be

$$\mathbf{x}(j) \cong \phi_d\lambda_{\max}^j a_d. \tag{14}$$

From the ratios $x_m(j+1)/x_m(j)$ for j large, we find $\lambda_{\max}$.

It is also possible to extend this conventional power method[16] to allow computation of all the eigenvalues and eigenvectors of $\mathbf{H}$ on the IOP as noted in Refs. 10 and 11. In practice, we normally use Eq. (9) to estimate $\lambda_{\max}$. Since the calculation of the Euclidean norm of $\mathbf{H}$ in Eq. (9) is easily achieved in the microprocessor system, and since the calculation need only be done once and the same acceleration parameter ω used for all iterations, the technique in Eq. (9) is used in preference to the one in Eq. (14). When ω is properly chosen, the system's iterative algorithm monotonically converges, and the stability of the algorithm and the IOP system are assured. This solution in Eqs. (8) and (9) has worked well for all vector–matrix and matrix–matrix problems to which we have applied the IOP. Even when the matrix is ill-conditioned, use of this acceleration parameter insures convergence of the algorithm, although many iterations may be required.

III. Bipolar and Complex-Valued Data

The LED and photodetectors outputs as well as the transmittances of the mask in the system of Fig. 1 must be real and positive. Since noncoherent light is used, the IOP cannot handle bipolar or complex-value data directly. This is a severe limitation of the system, and thus much work has been done to allow processing of such data on a vector–matrix system.[17] When the vector–matrix multiplier in Ref. 6 is used to compute the discrete Fourier transform of the spatial data present across the LED array, complex- valued data must be handled by the system. This is accomplished by formatting the input vector and the fixed elements of the matrix mask in terms of the bipolar real (Re) and imaginary (Im) parts of the vectors and matrix as

$$\begin{bmatrix} \mathbf{y}_{\mathrm{Re}} \\ \mathbf{y}_{\mathrm{Im}} \end{bmatrix} = \begin{bmatrix} \mathbf{H}_{\mathrm{Re}} & -\mathbf{H}_{\mathrm{Im}} \\ \mathbf{H}_{\mathrm{Im}} & \mathbf{H}_{\mathrm{Re}} \end{bmatrix} \begin{bmatrix} \mathbf{x}_{\mathrm{Re}} \\ \mathbf{x}_{\mathrm{Im}} \end{bmatrix}. \tag{15}$$

This requires $2M$ input LEDs, a $2M \times 2N$ mask, and a $2N$ element output detector. One can handle bipolar data on the system in many ways.[17] One technique that has been used[6] is to bias all vector and matrix elements so that they are positive. To obtain the bipolar vector–matrix product from the measured outputs, electronic postprocessing is needed. To perform this, additional factors such as the product of known bias matrices and the unknown input vector are necessary. These can be obtained by adding a column to the matrix mask at $\mathbf{P}_2$ that contains all constant elements and by including an additional detector element in the output.[17]

In our IOP we handle complex data as in Eq. (15), but we accommodate the bipolar data in Eq. (15) differently. We first decompose the bipolar input vector $\mathbf{x}$ into its positive $\mathbf{x}^+$ and negative $\mathbf{x}^-$ parts. The optical system's input vectors corresponding to each of these are $\mathbf{a}_1$ and $\mathbf{a}_2$, respectively, with elements

$$a_{1m} = 0.5(x_m + |x_m|) \qquad a_{2m} = -0.5(x_m - |x_m|). \tag{16}$$

The elements of the optical mask $\mathbf{B}$ are a scaled and biased version of the elements of the bipolar matrix $\mathbf{H}$. Specifically

$$b_{mn} = (h_{mn} - \underline{h})/(\overline{h} - \underline{h}), \tag{17}$$

where $\underline{h}$ and $\overline{h}$ are the minimum and maximum elements of $\mathbf{H}$. With the $\mathbf{P}_2$ mask described by Eq. (17), we see that the elements of B satisfy $0 \le b_{mn} \le 1$ as is necessary. We then achieve a bipolar vector–matrix multiplier by operating the system twice, once with $\mathbf{a}_1$ as the input vector and once with $\mathbf{a}_2$ as the input vector, with the same fixed $M \times N$ mask $\mathbf{B}$ present in both cases. The microprocessor forms the difference $\mathbf{Ba}_1 - \mathbf{Ba}_2$ between the system's outputs in the two cycles and scales and biases the difference according to

$$\mathbf{y} = \mathbf{Hx} = (\overline{h} - \underline{h})(\mathbf{Ba}_1 - \mathbf{Ba}_2) + \underline{h} \sum_m x_m(1, \ldots, 1)^T. \tag{18}$$

All the required operations in Eq. (18) are easily performed in the microprocessor support system since only additions, subtractions, and multiplications by fixed constants are required. The two-cycle algorithm in Eq. (18) by which bipolar data are handled on the IOP has two other attractive features worth noting. First, the size of the input LED array is only M (rather than $2M$) and the size of the output photodetector array is N (not $2N$). Likewise the matrix mask must be $M \times N$ (rather than $2M \times 2N$). Thus, larger vectors and matrices can be handled on a given system at the expense of using the two cycles of the system. Since the potential speed of the IOP is so high, trading a factor of 2 in speed for a factor of 2 or 4 in the sizes of the vectors and matrices that can be handled appears to be a useful trade off for the applications with which we are concerned. A second practical feature resulting from the use of the algorithm in Eq. (18) is that all fixed pattern detector noise is automatically cancelled. In Fig. 2 we show the system's outputs ($\mathbf{c}_1 = \mathbf{Ba}_1$ and $\mathbf{c}_2 = \mathbf{Ba}_2$) on two successive iterations with no input present (i.e., $\mathbf{a}_1 = \mathbf{a}_2 = 0$) and the electronically calculated difference $\mathbf{c}_1 - \mathbf{c}_2$. The outputs are thus caused by detector noise only. As seen in the $\mathbf{c}_1$ and $\mathbf{c}_2$ outputs, the detectors have a large leakage current ($\cong$8% of full scale) in a fixed spatial pattern. However, after subtraction all fixed pattern noise and leakage current effects are canceled (as is seen in the $\mathbf{c}_1 - \mathbf{c}_2$ difference output), and we are left with only the temporal noise variations (Johnson noise) of the detector. In Fig. 2, this noise is measured to be <0.4% of full scale.

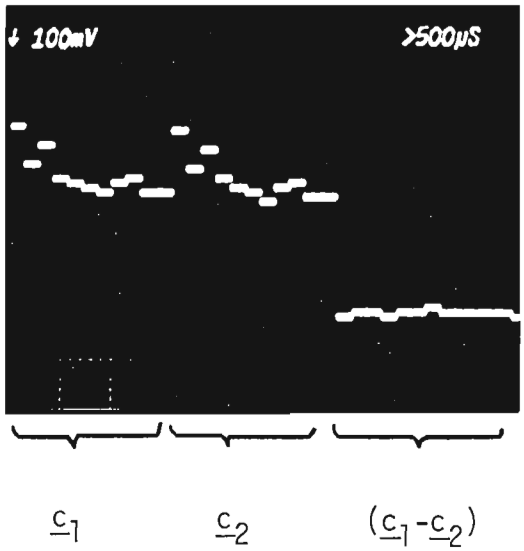

Fig. 2. Photodetector output $\mathbf{c}_1$ and $\mathbf{c}_2$ at two successive iterations and their difference showing suppression of detector leakage current and fixed-pattern noise.

IV. System Fabrication

Let us now consider the laboratory IOP system we fabricated with attention to the microprocessor system and the fiber-optic interconnections and how these features are used to overcome many potential system error sources. A detailed analysis of the system's error sources and quantitative data on the system's performance are included in Sec. V.

The electronic feedback system was to compute: the running iterative sum on the right-hand side of Eq. (3), the acceleration parameter ω in Eq. (9), the LED preprocessing in Eq. (16), the matrix scaling and biasing in Eq. (17), and the detector postprocessing in Eq. (18). It must also properly sync, control, and format the LED inputs and system cycling for bipolar and complex-value data handling. In practice, LED and photodetector correction factors are also included in the preprocessing and postprocessing (Sec. V). All these operations can be hard-wired and performed at high speed in a dedicated system. However, to enable the use of the IOP to be studied for many diverse problems and applications, a flexible rather than a dedicated electronic support system was desired. We achieved this with a microprocessor support system. A schematic of the IOP emphasizing the microprocessor electronic feedback and support system is shown in Fig. 3.

The electronic feedback system contains four subsystems:

(1) An LED board that performs the necessary preprocessing in Eq. (16) for handling bipolar and complex-valued data, provides the multiplexed pulsewidth-modulated current drive for the LEDs and corrections for nonuniform LED saturation levels.

(2) A detector board with parallel resettable operational–amplifier (op–amp) integrators to allow variable detector integration times and correction for nonuniform photodiode responsivity.

(3) Analog to digital (ADC) and digital to analog (DAC) converters for input to and output from the microprocessor controller.

(4) a microprocessor controller subsystem. This controls the scheduling of all IOP operations and performs the operations in Eqs. (3), (9), (17), and (18). The microprocessor subsystem contains a control section with a Fairchild 9408 LSI microprogram sequencer to execute various microprograms stored in a 26K random access memory (RAM) program memory and a thirty-two line instruction decoder to activate various control points in the system. It also contains an arithmetic data section containing a custom-designed arithmetic unit consisting of a 16-bit 300-nsec multiplier, a 16-bit arithmetic logic unit (ALU), and a 16K RAM with a special row-column address structure. In this data section all arithmetic operations are performed at high speed. The 16K RAM is used to store fixed data such as LED and photodetector response correction factors ω, $(\bar{h} - \underline{h})$, etc. The system is also provided with a capability of storing up to fifty-four different selected iterative data outputs for future display on a scope or for input to a microcomputer for analysis. The laboratory IOP system also contains a front panel console from which the operator can load any programs into the 26K or 16K memory depending on the IOP application being considered. It also includes all necessary operator controls to start, stop, and reset the microprocessor IOP.

A photograph of the full microprocessor-based IOP is shown in Fig. 4. The front panel is shown at the top. Below this is the microprocessor system. The optical

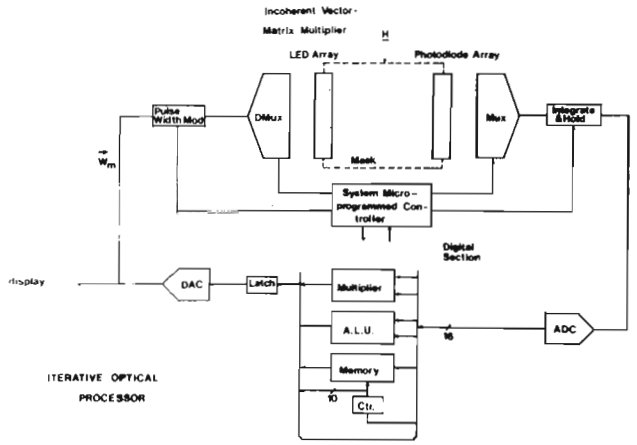

Fig. 3. Schematic diagram of the IOP emphasizing the microprocessor-based electronic support system.

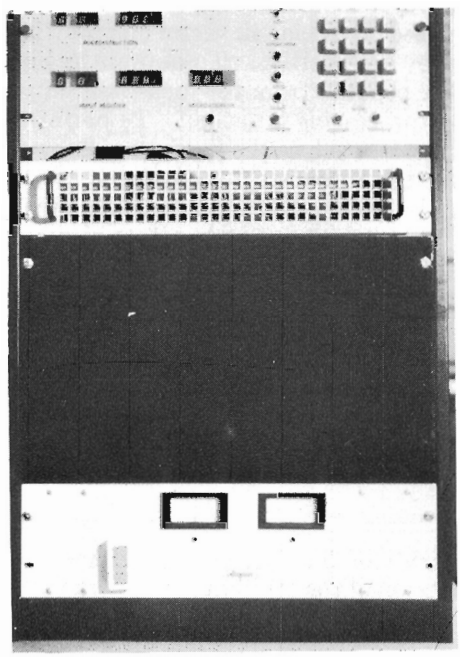

Fig. 4. Laboratory IOP and its entire electronic support system (microprocessor, power supply, front panel console).

IOP system is placed behind the central dark panel, and the system's power supplies are on the bottom of the rack. The present electronic support system contains 160 integrated circuits, requires 50 W of power, and has a 300-nsec cycle time. Higher speed is possible, but the flexibility and cost of the assembled system just described were more compatible with our goals. Moreover, it provided us with a sufficiently powerful system to be used on many different applications and problems, and sufficient complexity to allow unforeseen problems in the design and fabrication of larger systems to be uncovered.

The laboratory IOP system uses a linear input array of ten RCA SG-1002 LEDs at plane $\mathbf{P}_1$ of Fig. 1 with 1-mW output at 940 nm for a 50-mA drive current. The LEDs are mounted on 0.375-cm centers along a copper block 3.75 cm long. They are held in place by silver epoxy and sealed in white RTV compound. The inner connections from $\mathbf{P}_1$ to the mask at $\mathbf{P}_2$ are accomplished by a specially fabricated fiber-optic system. It contains a linear array of ten apertures at one end into which the LEDs are placed. Each aperture contains ten glass fibers, each 25 μm in diameter, that branch outward to form a line of ten fibers. The output from the fiber-optic system is thus a 10×10 array of 100 fibers whose locations match the 10×10 elements of the mask at $\mathbf{P}_2$. The fiber outputs have a center-to-center spacing of 0.35 mm vertical and 0.94 mm horizontal. The $\mathbf{P}_2$ mask is placed between these fiber-optic outputs in the detector array. In the present system, the mask used is a fixed pattern recorded on film. An advanced IOP system we are presently designing will use a real-time light modulator (such as the CCD-addressed liquid crystal light valve[18]) as a real-time adaptive mask element. The detector used in the present system is a Centronics LD-20 silicon photodiode array containing twenty elements each measuring 4×0.9 mm on 0.94-mm centers. The spacings and sizes of the outputs from the fiber-optic system were chosen to match the size of the elements in this detector. The horizontal spacing between fibers equals the spacing between detector elements, and the height of the ten vertical fiber outputs equals the height of a detector element. This allowed us to sandwich the mask between the output from the fiber-optic element and the detector with no imaging optics necessary between $\mathbf{P}_2$ and $\mathbf{P}_3$ in Fig. 1. A photograph of the optical vector–matrix multiplier is shown in Fig. 5. From right to left are the LED array, fiber-optic connector, mask, and photodetector array. The photodetector board is also visible on the left. The components in the system have been separated for clarity in the photograph. In practice, the entire system is less than 5 cm long.

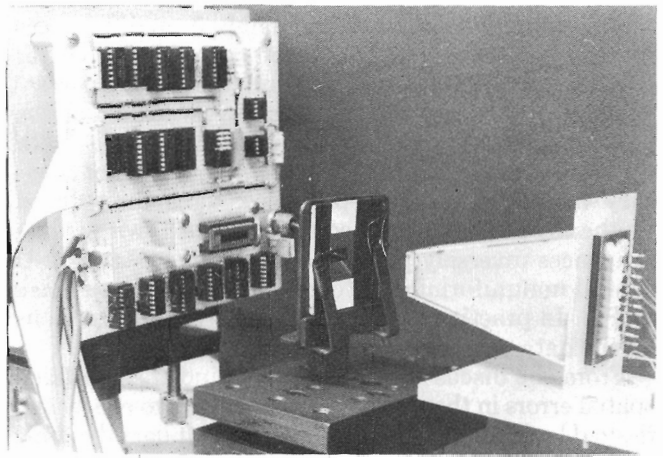

Fig. 5. Laboratory optical vector–matrix multiplier.

V. System Performance

In this section we discuss the performance of the laboratory IOP system we fabricated and emphasize how many system designed features were chosen to improve the accuracy and stability of the system. The first IOP that we fabricated[9] used cylindrical lenses for imaging from $\mathbf{P}_1$ to $\mathbf{P}_2$ and from $\mathbf{P}_2$ to $\mathbf{P}_3$. Experiments and simulation analysis on this system showed that two major error sources were cross talk in the vertical imaging from $\mathbf{P}_1$ to $\mathbf{P}_2$ and nonuniform illumination of each row of the $\mathbf{P}_2$ mask. The fiber-optic system (Sec. IV) effectively removes both of these error sources. Similar problems were found to occur in the required imaging from $\mathbf{P}_2$ to $\mathbf{P}_3$. By placing the detector, mask, and fiber-optic element in contact, these error sources were similarly removed, and a rugged stable system (Fig. 4) of greatly reduced size and weight resulted.

Amplitude nonlinearities in the light outputs from the LEDs is a well-known problem. These components are thus usually operated at a fixed bias current and amplitude-modulated over a restricted range to decrease nonlinear effects. This results in a decreased useful linear dynamic range. Correction for LED nonlinearities is possible but was not included in the laboratory system. Rather, we use pulse width modulation (PWM) of the LEDs when linear performance and large dynamic range data are needed. When operated in the PWM mode, the present laboratory system has a minimum to maximum pulse-width ratio of 256 and thus a 256:1 input dynamic range. This has proven adequate for all applications with which we are concerned. Use of laser diodes rather than LEDs for the input source array allows amplitude modulation with a large linear dynamic range. However, linear laser diode arrays are not yet commercially available, and thus our present system is operated with an LED input source array.

When operated in the PWM data mode, a large spatial nonuniformity in the output power from the LEDs of $\pm 25\%$ was measured. This fixed error is corrected for by multiplying the input signal to the mth LED by the reciprocal of its response. Spatial nonuniformities of $\pm 7\%$ were measured for the responsivity of the output photodetector elements. These output nonuniformities were similarly corrected for by multiplying each photodiode output by its appropriate reciprocal responsivity correction factor. These multiplicative source and detector corrections are directly included in the preprocessing and postprocessing with no additional overhead, since the correction factors can be measured once and stored in the microprocessor system's 16K data memory. As noted in Sec. III, the bipolar data handling algorithm in Eq. (18) automatically cancels all fixed-pattern detector noise and detector leakage current effects.

Residual spatial nonuniformity errors caused by the source and detector may still remain. In addition, differences in the coupling loss from the different LEDs to the different fiber-optic elements may exist together with spatial variations in the outputs from the 100

fiber-optic elements (resulting mainly from differences in the polishing of the ends of each fiber). After applying the preliminary LED and photodiode corrections, we measured the 2-D spatial variations of the entire system and found a residual nonuniformity with a standard deviation of only 0.8%. This level of accuracy was sufficient for our purposes. It can be reduced further by placing a fixed correction mask (with transmittances inversely proportional to the system's 2-D spatial nonuniformity) in contact with the data mask at $\mathbf{P}_2$. In practice, we include these fixed corrections on the data mask itself when it is recorded.

From the discussion thus far, we find that all fixed spatial errors in the system can be reduced to nearly any desired level, and nearly any desired input data dynamic range can be achieved (by pulse width modulation with an associated loss in speed, by amplitude modulation of a laser diode source array, or by a combination of amplitude and PWM modulation). The major errors in the system are thus the time-varying thermal noise in the detector, and noise in the data recorded on the mask at $\mathbf{P}_2$. In the present system, the temporal detector noise is <0.4% of full scale. This can be further reduced by use of cooled detectors, advanced detector fabrication techniques, and chopper-stabilized operational amplifiers if necessary. Noise in the recorded data at $\mathbf{P}_2$ thus appears to represent the major limitation in the system's performance. A general analysis of the effect of this error source on the performance of the iterative algorithm is not possible. Rather, specific case studies and applications must be individually addressed. In general, we have found that the accuracy of the final answer in the iterative algorithm will be less than or equal to the error in a given vector–matrix product with final errors of 1% being quite easily achieved. In some cases, the $\mathbf{P}_2$ matrix mask can be row or column biased to reduce its dynamic range requirements. Such issues are best treated for specific applications. We are in the process of completing such analyses for adaptive phased array radar[9] and linear quadratic regulator control[12] applications on the IOP. These will be published and this issue addressed more fully when sufficient data and funding are available.

VI. Summary and Conclusion

In this paper, we have described the design and fabrication of an iterative optical vector–matrix processor and the performance possible from such a system. The use of a microprocessor electronic support system was shown to provide extensive flexibility in the laboratory system assembled. The use of fiber-optic interconnections was found to result in a rugged and stable system of small size and weight and remove cross talk and nonuniform illumination error sources. A new algorithm for handling bipolar data on the system was shown to provide cancellation of spatial fixed-pattern system noise. Source and detector nonuniformities are also easily corrected by RAM look-up tables. The residual spatial system error on the laboratory IOP assembled was <0.8%, and its temporal noise was below 0.4%.

This present system description has only emphasized its use in solving linear algebraic equations or vector–matrix equations. In Sec. II we noted that the system can also be used to compute the eigenvalues and eigenvectors of a matrix. Multiplication of two $M \times M$ matrices is also possible on the system by vectorizing one matrix or by running the system M times with the M columns of one matrix as inputs. Matrix inversion is similarly possible by describing the problem as N problems each of the form of Eq. (3) with $\mathbf{y} = 1$. We have also[12] used the system to solve nonlinear matrix–matrix problems using a modified Newton-Rhapson algorithm. In this latter application the solution involves an inner and an outer iterative loop, with the output from the inner loop fed to the outer loop after N iterations and a different mask necessary for each outer loop iteration. The IOP system thus appears to be a viable, powerful, flexible, and quite general purpose processor with many potential applications.

The authors thank Rome Air Development Center for initial support of this research, Air Force Office of Scientific Research (grant 79-0091) for interim support, and NASA Lewis Research Center (grant NAG 3-5) for present support of our IOP research.

References

1. L. Cutrona, in *Optical and Electro-Optical Information Processing*, J. Tippett *et al.*, Eds. (MIT Press, Cambridge, 1965), pp. 97–98.
2. A. Edison and M. Noble, Optical Analog Matrix Processors, A. D. 646060 (Nov. 1966).
3. P. Mengert *et al.*, U.S. Patent 3,525,856 (6 Oct. 1966).
4. M. Monahan, in *Digest of the International Optical Computing Conference*, IEEE Catalog 75-CH0941-5C (IEEE, New York, 1975), pp. 25–33.
5. M. Monahan, K. Bromley, and R. Bocker, Proc. IEEE **65,** 121 (1977).
6. J. W. Goodman, A. R. Dias, and L. M. Woody, Opt. Lett. **2,** 1 (1978).
7. J. Goodman *et al.*, Proc. Soc. Photo-Opt. Instrum. Eng. **190,** 484 (1979).
8. D. Psaltis, D. Casasent, and M. Carlotto, Opt. Lett, **4,** 348 (1979).
9. D. Psaltis *et al.*, Proc. Soc. Photo-Opt. Instrum. Eng. **180,** 114 (1979).
10. H. J. Caulfield, D. Dvore, J. W. Goodman, and William Rhodes, Appl. Opt. **20,** 2263 (1981).
11. B. Kumar and D. Casasent, Appl. Opt. **20,** 3707 (1981).
12. D. Casasent *et al.*, Proc. Soc. Photo-Opt. Instrum. Eng. **295** (1981).
13. L. F. Richardson, Philos. Trans. R. Soc. London, Ser. A **210,** 307–357 (1910).
14. E. Jury, *Theory and Applications of the z-Transform Method* (Kreiger, New York, 1973).
15. E. Kreyszig, *Advanced Engineering Mathematics* (Wiley, New York, 1972).
16. G. Stewart, *Introduction to Matrix Computations* (Academic, New York, 1973).
17. J. Goodman *et al.*, "Incoherent Optical Matrix-Vector Multiplier," Stanford U. Tech. Rept. L-723-1 (Feb. 1979).
18. J. Grinberg *et al.*, Proc. Soc. Photo-Opt. Instrum. Eng. **128,** 253 (1977).